Electronic structure of low-carrier Yb_4As_3 and related compounds

V. N. Antonov,* A. N. Yaresko,* A. Ya. Perlov,* P. Thalmeier,† and P. Fulde
Max Planck Institute for the Physics of Complex Systems, D-01187 Dresden, Germany

P. M. Oppeneer and H. Eschrig
Institute of Theoretical Physics, University of Technology, D-01062 Dresden, Germany
(Received 22 January 1998)

The electronic structure of the heavy-fermion compound Yb_4As_3 is investigated using energy band calculations within the so-called local spin density approximation+U approach. We find as a generic feature a very rigid pinning of the energy of Yb $4f$ hole states close to the top of the pnictide p band and the Fermi level pinned to those hole states, providing for a very low-carrier concentration. Calculated Fermi surface and optical properties compare well with experimental data. We also present electronic structure results for the related compounds Yb_4P_3, Yb_4Sb_3, Yb_4Bi_3, and $Yb_4(P_{0.5}As_{0.5})_3$.
[S0163-1829(98)03636-4]

I. INTRODUCTION

The rare-earth pnictides Yb_4X_3 (X=P, As, Sb, Bi) exhibit unusual physical properties.[1–8] The high-temperature phases of these compounds have the cubic anti-Th_3P_4 structure with space group $I4\bar{3}d$. The Yb ions occupy the P sites with Wyckoff positions 12*a*, $\bar{4}$.., $x=0.069$, and the X ions occupy the Th sites with special Wyckoff positions 16*c*, .3., fixed by symmetry[9] [see Fig. 1(a)]. All Yb atoms are aligned on four families of chains oriented along the four diagonals of the cubic unit cell [see Fig. 1(b)].[10] All four ytterbium pnictides have anomalously large lattice constants (a =8.56, 8.788, 9.322, and 9.573 Å for X=P, As, Sb, and Bi, respectively).[1,2] Because the pnictide ion is trivalent, three of the four Yb ions have a filled $4f$ shell (valency 2+) while one ion is in a $4f^{13}$ (valency 3+) configuration. When all Yb sites are equivalent, the hole in the $4f$ shell is moving between different Yb ions and the system is a mixed valent metal. Its average Yb valence $Z=2.25$ is rather close to the observed one ($Z_{\rm exp}$=2.20), obtained from Mössbauer experiments.[3]

The most interesting material is Yb_4As_3. At about T_s =300 K it undergoes a weak first-order phase transition with a trigonal distortion. This transformation was clearly established by susceptibility measurements,[1] Mössbauer spectra,[3] polarized neutron diffraction,[11] and elastic constant measurements.[12] At the structural transformation, the crystal shrinks in a volume-conserving way along one of the four Yb-chain directions ($\langle 111\rangle$, say). The resulting trigonal unit cell with the trigonal angle $\alpha=90.8°$ has the *short chain* along its main axis. The centered trigonal space group is now $R3c$ with two inequivalent Yb sites at Wyckoff positions 2*a*, 3., and two further inequivalent Yb sites at Wyckoff positions 6*b*, 1, as well as two inequivalent As sites at Wyckoff positions 6*b*, 1. The parameters used in our calculations are specified below in the paragraph before last of Sec. II. The distortion is accompanied by charge ordering with Yb^{3+} ions occupying the short chains. So the $4f$ electronic state of Yb_4As_3 changes from a valence fluctuating state in the cubic phase to a charge-ordered state $Yb^{3+}Yb_3^{2+}As_3^{3-}$ in the trigonal phase, although the charge ordering is not complete.[3,11] The Yb^{2+} ions have a closed $4f$ shell with no spin magnetic moment. The Yb^{3+} ions have the $4f^{13}$ configuration with nominal spin magnetic moment equal to one. Inelastic neutron scattering experiments on Yb_4As_3 revealed the existence of low-energy excitations that are characteristic of a one-dimensional antiferromagnetic coupling at low temperatures.[11]

Below 100 K, Yb_4As_3 exhibits heavy-fermion behavior: the resistivity shows a T^2 behavior ascribed to electron-electron interactions involving the heavy-quasiparticle band, the Sommerfeld coefficient γ of the electronic specific heat C_{el} has a relatively high value of about 200 mJ mol^{-1} K^{-2}, and the extrapolated magnetic susceptibility at 0 K has a rather large value $\chi(0)\simeq 3\times 10^{-2}$ emu/mol (Ref. 1). The Sommerfeld-Wilson ratio is found to be of the order of unity, indicating Fermi-liquid behavior. Below 2 K and for moderate applied magnetic fields (>2 T), the ''high field'' magnetic susceptibility of Yb_4As_3 drops considerably as compared to the low field value.[13] There is also a rapid decrease observed in the specific heat at an applied field of about 1 T,[4] both observations indicating the destruction of the heavy electron behavior.

The Hall coefficient R_H of Yb_4As_3, extrapolated to T =0, is equal to 7×10^{18} cm^{-3} (see Ref. 1). It would correspond to a carrier concentration of about 0.001 per formula unit if only one type of carriers was present.

The pressure effects on transport properties of Yb_4As_3 were investigated by Okunuki *et al.*[14] and by Mori *et al.*[15] A clear increase of the carrier concentration is observed with increasing pressure, which leads to a rapid decrease of the resistivity ρ. The maximum in the temperature dependence of both ρ and R_H also decreases with pressure. However, the inverse Hall mobility, i.e., the resistivity divided by the Hall coefficient, is found to increase with increasing temperature without any anomaly in the low-temperature phase even under high pressure. This demonstrates that the mobility is not affected by pressure.

The effect of doping on physical properties of Yb_4As_3 has been investigated by means of substitution of As with P[16,2] or with Sb.[17] According to the temperature dependence of the Hall constant and of the resistivity, the $Yb_4(P_xAs_{1-x})_3$

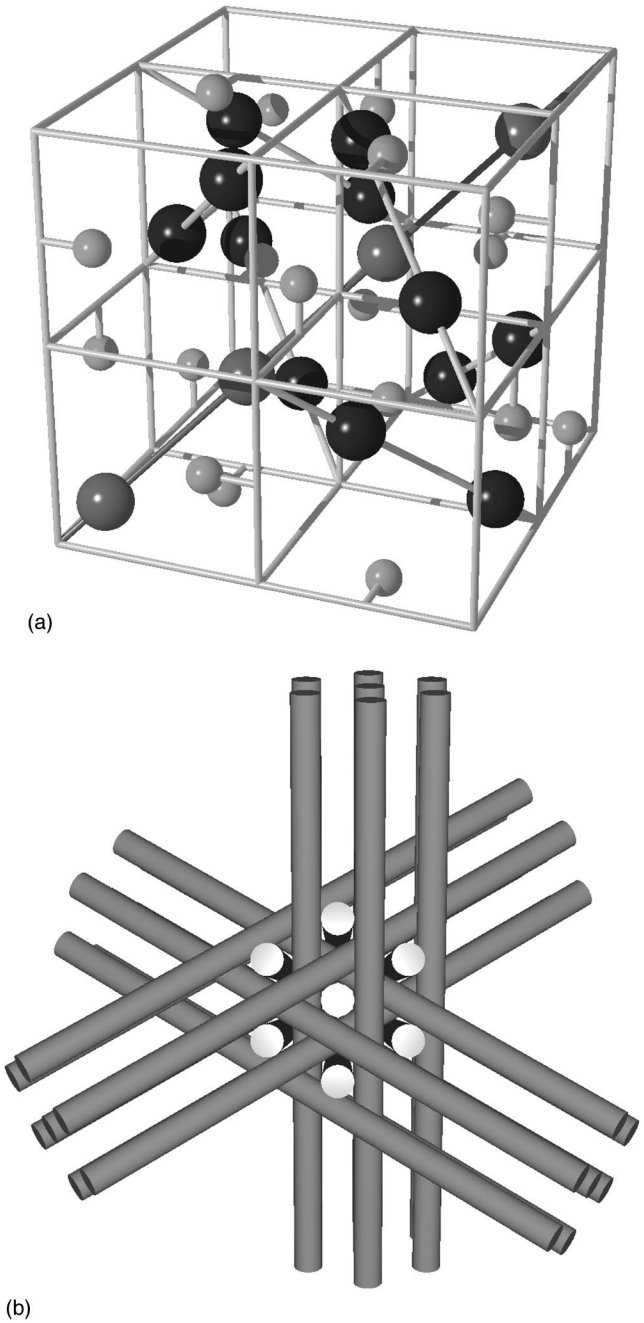

FIG. 1. (a) Structure of Yb_4X_3. Large balls: Yb ions, small balls: pnictide ions. In the trigonal charge-ordered phase the black large balls indicate Yb^{2+} sites and the gray large balls Yb^{3+} sites. (b) The four families of chains formed by the Yb atoms.

system becomes semiconducting for higher concentration of phosphorus. However, the specific heat and magnetic susceptibility are almost the same as those of pure Yb_4As_3. Recent measurements[18] have shown that the temperature dependences of the magnetic susceptibility and the specific heat of pure Yb_4P_3 exhibit almost the same behavior as those of Yb_4As_3 below the charge-ordering temperature T_s, but above T_s the susceptibility is about two times larger, indicating an increase of the fraction of Yb^{3+} ions in the high-temperature phase. The γ value is also large, about 250 mJ mol^{-1} K^{-2}, and the behavior of Yb_4P_3 in an external magnetic field is very similar to that of Yb_4As_3.

The temperature dependence of the Hall coefficient and the electrical resistivity in the $Yb_4(As_{1-x}Sb_x)_3$ system shows[17] that with increasing concentration of Sb the number of carriers increases. From $x=0$ to $x=0.12$, the heavy fermion behavior is little affected by the increase of the carrier concentration. In $Yb_4(As_{0.71}Sb_{0.29})$, however, no clear evidence of charge ordering is observed anymore, and in pure Yb_4Sb_3 there is no evidence of the ordered state, and a proper γ value of about 40 mJ mol^{-1} K^{-2}, corresponding to the valence fluctuation state, is observed.

It was also revealed that Yb_4As_3 shows a strong sample dependence of the transport properties.[19]

Summarizing all the experimental data, we can conclude that there is a strong dependence of the transport properties of Yb_4As_3 on doping, pressure and sample preparation, but the specific heat and magnetic susceptibility do not change very much. This observation suggests that Yb_4As_3 is not an ordinary heavy-fermion system. The latter are usually interpreted within the context of a Kondo lattice model: The heavy quasiparticle bands are thought to originate from Kondo resonance states at the Fermi level, which evolve into coherent band states below a characteristic temperature. However, this mechanism leads to a similar behavior of the specific heat coefficient γ and of the carrier number as functions of doping. As explained above, the opposite behavior is observed, which is a strong argument against the Kondo scenario in this class of compounds.

The electronic structure of Yb_4As_3 has been investigated experimentally by means of photoemission,[20,21] x-ray bremsstrahlung isochromat spectroscopy[22] (BIS), optical properties,[23–26] and cyclotron resonance measurements.[27] The optical measurements[23,24,26] show a strong temperature dependence of the optical reflectivity in the far infrared energy region below 10 meV. The plasma frequency ω_p derived from optical measurements[25] is very small. It varies from 0.08 eV for 10 K to 0.14 eV for 70 K, indicating again an extremely small carrier number. Photoelectron spectroscopy in the x-ray and ultraviolet ranges (XPS and UPS) provide information on the energy position of Yb^{2+} and Yb^{3+} $4f$ states in charge ordered Yb_4As_3. Structures in UPS and XPS spectra with binding energy between 0 and 4 eV were identified[20,21] to be the spin-orbit doublet of the $4f^{13}$ final states and the structures between 6 and 13 eV to be the multiplet structures of the $4f^{12}$ final states. The low-temperature photoemission also does not show any evidence for Kondo resonance states close to the Fermi level, confirming the exclusion of the Kondo scenario for Yb_4As_3. Cyclotron resonance measurements[27] yield a single rather small cyclotron mass of $0.72m_0$.

Energy band structure calculations for anti-Th_3P_4 type rare-earth pnictides were performed first for La_4Sb_3 and La_4Bi_3,[28] and later on for Yb_4As_3.[29] The calculations of Ref. 29 were done by means of the self-consistent augmented plane wave (APW) method on the basis of the local density approximation (LDA) and for the cubic $I4\bar{3}d$ crystal structure. The calculations were able to reproduce the main features of BIS, originating from the Yb $5d$ states, but failed to reproduce the correct position of the f band due to the strongly correlated nature of the $4f$ electrons in Yb_4As_3. The calculations obtain the $4f$ bands at the Fermi level. From the

band structure results for the cubic phase it was conjectured that Yb_4As_3 should be an insulator in the charge-ordered phase. Recently, non-spin-polarized LDA band-structure calculations of Yb_4As_3 and $LuYb_3As_3$ in both the cubic and trigonal crystal structures were reported.[30] The calculations were carried out using the linearized APW method with scalar relativistic effects being included for all electrons, and the spin-orbit interaction was included for valence electrons by a second variational procedure. It was found for a hypothetical $LuYb_3As_3$ system that the top of the As p band and the bottom of the Lu d band cross the Fermi energy ϵ_F. The $4f$ states are fully occupied due to the $3+$ valency of the Lu ion, and are positioned close to ϵ_F. The cyclotron mass of the largest hole Fermi surface was calculated to be $0.7m_0$, which is in good agreement with cyclotron resonance measurements.[27]

Two approaches have been proposed to explain the properties of Yb_4As_3. One is based on a one-electron picture and was applied by Ochiai *et al.*[1] in the form of a four-band model and by Kasuya[31] in the form of a two-band model. A characteristic feature of this approach is a hole band of As $4p$ states and an Yb $4f$ band with a high density of states near the Fermi level. The second approach treats the $4f$ electrons as being strongly correlated.[32–34] Charge ordering of the Yb^{3+} ions and the associated structural phase transition are a consequence of reducing the sum of the Coulomb repulsion and exchange to a minimum, and are described by a band Jahn-Teller effect of correlated electrons. The observed heavy-fermion behavior is ascribed to spinlike excitations in the Yb^{3+} chains.

The aim of this paper is to combine the two approaches by studying the electronic structure and the physical properties of Yb_4As_3 in the trigonal low temperature $R3c$ phase within an *ab initio* band-structure approach that takes strong correlations into account. This is achieved by applying a local spin density approximation (LSDA) to the density-functional theory supplemented by a Hubbard U term (LSDA$+U$). We also consider the electronic structure of the related compounds Yb_4X_3 ($X=$ P, Sb, Bi, and $P_{0.5}As_{0.5}$).

The paper is organized as follows. The theoretical approach and the computational details are explained in Sec. II. Section III presents the electronic structure of Yb_4As_3 calculated in both the LSDA and the LSDA$+U$ approach. The results are compared to UPS measurements, optical spectra, and cyclotron resonance measurements. The energy band structures of Yb_4P_3, $Yb_4(P_{0.5}As_{0.5})_3$, Yb_4Sb_3, and Yb_4Bi_3 are presented, as well as the dependence of the energy band structure of Yb_4As_3 on the lattice spacing. The charge ordering is studied by total energy calculations. Finally, the results are summarized in Sec. IV.

II. COMPUTATIONAL APPROACH

The application of plain LSDA calculations to f-electron systems is often inappropriate, because of the correlated nature of the f shell. To account better for the on-site f-electron correlations, we have adopted as a suitable model the LSDA$+U$ approach. There are attempts in the literature to base this approach on heuristic arguments, observing a certain similarity to self-interaction corrections (SIC) to the LSDA (Ref. 35) and a certain link to the self-energy of the single-particle Green's function.[36]

SIC (Ref. 37) adds an orbital-dependent potential correction term to the Kohn-Sham equation, which results in a downshift of Kohn-Sham orbital energies of localized orbitals. For localized $4f$ orbitals this shift is of the order of 10 eV. The $4f$ orbitals themselves are slightly squeezed by this potential correction, but mainly the ground-state density calculation is brought into accord with Janak's theorem.[38] Recall that Janak's theorem states that $\partial E/\partial n_m=\epsilon_m$ equals the Kohn-Sham orbital energy, if the energy functional E is expressed through the true Kohn-Sham orbitals ϕ_m and orbital occupation numbers n_m via the density expression $n=\Sigma n_m|\phi_m|^2$. This entails the occupation rule that in the ground state orbitals are occupied in the order of ascending Kohn-Sham energies.[39] It does *not* entail that the Kohn-Sham energies describe the quasiparticle excitation spectrum.

The self-energy $\Sigma=G_0^{-1}-G^{-1}$ of the single-particle Green's function G is energy dependent and yields the correlation corrections to the single-particle (mean-field) approximation to the quasiparticle excitation spectrum described by G_0. With a number of plausible assumptions, the LSDA$+U$ approach has been related to the so-called GW approximation to Σ in Ref. 36. Already the simplest random phase approximation applied to Σ for the Hubbard model yields a jump of $\Sigma(\epsilon)$ at the Fermi level ϵ_F by the Hubbard U. The more elaborate analysis of Ref. 36 results in a correlation correction to the mean-field approximation of the self-energy, which is $U_{\rm eff}/2$ downward below the Fermi level and $U_{\rm eff}/2$ upward above the Fermi level. As the mean-field theory in a crystal describes always a delocalized situation and the LSDA Kohn-Sham potential is a well-proved approximation to the self-energy of weakly correlated electrons,[40] the suggestion is

$$\Sigma(\boldsymbol{r},\boldsymbol{r}';\epsilon)\approx\delta(\boldsymbol{r}-\boldsymbol{r}')v_{\rm LSDA}(\boldsymbol{r}) + P_m\frac{U_{\rm eff}}{2}[\theta(\epsilon-\epsilon_F)-\theta(\epsilon_F-\epsilon)]P_m, \quad (1)$$

where P_m is the projector onto a strongly correlated m state.

The LSDA$+U$ approach simply uses Eq. (1) to replace the LSDA Kohn-Sham potential in the self-consistency loop. This can be considered as a rough approximation to both SIC and Σ. Since the potential shift is taken to be constant in space, it does not deform the Kohn-Sham orbital ϕ_m as the $\boldsymbol{r}$-dependent SIC potential of Ref. 37 does. However, it shifts the levels of strongly correlated electrons away from the Fermi level and thus removes incorrect hybridization with conduction states, which would spoil the calculated ground-state spin density. On the other hand, being also understood as an approximation to Σ, it hopefully yields for the Kohn-Sham band structure the same quality of a working approximation to the quasiparticle excitation spectrum as it does in the case of weakly correlated metals. Estimates for $U_{\rm eff}$ may be obtained from constrained density-functional calculations or from GW calculations in which case the approach is parameter-free. Most reliable are those results that do not very sensitively depend on the actual value of $U_{\rm eff}$ within a certain reasonable range.

The LSDA+U method has proved to be an efficient and reliable tool for calculating the electronic structure of systems where the Coulomb interaction is strong enough to cause localization of the electrons. It works not only for nearly corelike $4f$ orbitals of rare-earth ions, but also for such systems as transition-metal oxides, where $3d$ orbitals hybridize quite strongly with oxygen $2p$ orbitals (for a review see Ref. 36). The LSDA+U approach was recently applied to the heavy-fermion compound YbPtBi,[41] and also to explain the nature of the maximal possible polar Kerr rotation of 90° in CeSb (see Ref. 42).

In the present work, self-consistent energy band-structure calculations of Yb_4As_3 were performed by means of the spin-polarized fully relativistic linear muffin-tin orbital (SPR LMTO) method in spherical potential approximation with combined corrections included,[43–45] for both cubic $I4\bar{3}d$ and trigonal $R3c$ crystal structures. The LSDA part of the calculations was based on the spin-density functional with the von Barth–Hedin parametrization[46] of the exchange-correlation potential. Core-charge densities were recalculated at every iteration of the self-consistency loop. In the case of the $R3c$ structure we neglect the incompleteness of the charge ordering and assume antiferromagnetic (AF) order of the Yb^{3+} ions in the chains along the trigonal axis ($\langle 111\rangle$-chains of the high-temperature cubic $I4\bar{3}d$ reference structure). We also neglect the small trigonal distortion for simplicity and determined all positions in such a way that there is no ion displacement at all in the cubic to trigonal transformation. Instead the Yb f charges are redistributed by fixing which Yb site is $3+$ and which is $2+$, both cases treated differently with respect to the Hubbard U (see the next section). We checked that this neglect of ion displacements makes very little differences in our results. It should be mentioned that if we neglect the trigonal distortion, the LSDA (without U) band-structure calculations should give exactly the same results as for the cubic structure. That the effect of distortion on the LSDA band structure is negligible was recently also numerically confirmed by Harima.[30]

The $\boldsymbol{k}$-integrated functions, the charge density, the density of states (DOS), and the l-projected DOS were calculated by the improved tetrahedron method[47] on a grid of 252 and 924 $\boldsymbol{k}$ points in the irreducible part of the Brillouin zone (BZ) of the cubic and the trigonal systems, respectively (Fig. 2). The Fermi surface, the angular dependence of the extremal cross-sectional areas, and cyclotron masses were also calculated by a tetrahedron method[48] using a grid of 3781 $\boldsymbol{k}$ points in the irreducible part of the BZ.

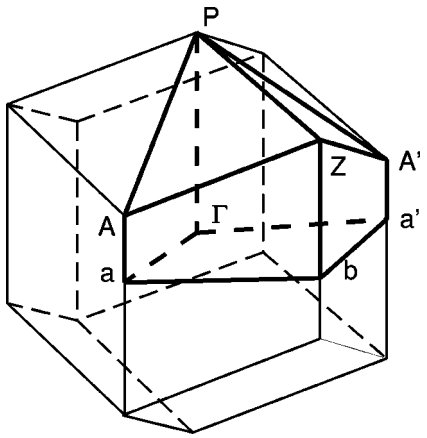

FIG. 2. Brillouin zone with symmetry points and axes of the trigonal $R3c$ symmetry group.

III. RESULTS AND DISCUSSION

A. Energy band structure of Yb_4As_3

The LSDA total DOS of Yb_4As_3 is shown in Fig. 3. These results agree well with previous band-structure calculations by Takegahara and Kaneta[29] and by Harima.[30] The occupied part of the valence band can be subdivided into three regions separated by energy gaps. The bands in the lowest region have mostly As s character with some amount of Yb s character mixed in. The next group of bands is formed by As p states with little admixture of Yb p and d states. The large narrow peak close to the Fermi energy is formed by Yb $4f$ states. Unoccupied $5d$ bands of Yb are separated from the $4f$ states by an energy gap, a characteristic and important feature of the ytterbium pnictides. The position of the LSDA $4f$ states close to the Fermi energy is, on the other hand, in contradiction to the findings of XPS and UPS experiments.[20,21]

In our SPR LMTO LSDA+U band-structure calculations we start from the $4f^{14}$ configuration for three Yb^{2+} ions, where all 14 on-site $4f$ energies are shifted downwards by $U_{\mathrm{eff}}^{(2+)}/2$, and from the $4f^{13}$ configuration for one Yb^{3+} ion with 13 on-site $4f$ energies shifted downwards by $U_{\mathrm{eff}}^{(3+)}/2$ and one level shifted upwards by this amount. From total energy calculations we found that the Yb^{3+} ground state corresponds to the projection of the orbital momentum onto the spin direction equal to $m_l=+3$ in accordance with all three Hund's rules. The energies of occupied and unoccupied Yb^{3+} f bands are separated by approximately $U_{\mathrm{eff}}^{(3+)}$. We emphasize, however, that the $4f$ states are not treated as completely localized. They may hybridize, and together with all other states their energy positions relax to self-consistency.

Usually the Hubbard-like U_{eff} is estimated by comparing the theoretically calculated energy positions of f bands with XPS and UPS measurements. In our particular case we have two types of Yb ions with different occupation numbers of

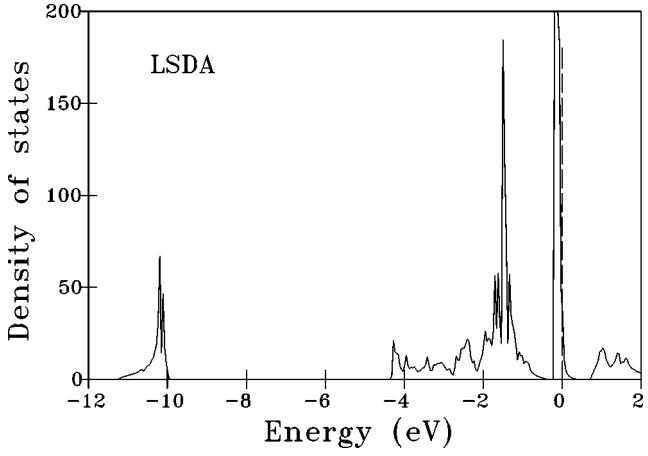

FIG. 3. LSDA total DOS of Yb_4As_3 in states per cell and eV.

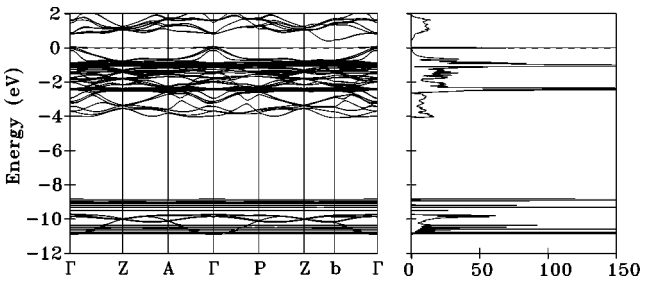

FIG. 4. Self-consistent LSDA+U energy band structure and total DOS per unit cell and eV of Yb_4As_3. ($U_{\rm eff}^{(2+)}$=5.3 eV, $U_{\rm eff}^{(3+)}$ =8.8 eV.)

their $4f$ shell. Obviously, the effective repulsion of $4f$ electrons $U_{\rm eff}$ depends on the number of holes in the $4f$ shell or the ionicity of the Yb ion,[49] and it should increase with increasing ionicity. From photoemission measurements $U_{\rm eff}$ is found to be in the range of 5–7 eV for different Yb compounds.[49] It can also be calculated from atomic Dirac-Hartree-Fock (DHF) calculations,[49] from Green's-function impurity calculations,[50] and from band-structure calculations in supercell approximation.[51] The DHF calculation gives $U_{\rm eff}\approx$5.3 eV and our calculations of $U_{\rm eff}$ in supercell approximation give $U_{\rm eff}$=8.4 eV. The calculated value of $U_{\rm eff}$ strongly depends on theoretical approximations and we prefer to treat the value of $U_{\rm eff}$ as a parameter and try to specify it from comparison of the calculated physical properties of Yb_4As_3 with experiments.

The LSDA+U energy bands of AF Yb_4As_3 for $U_{\rm eff}^{(2+)}$ =5.3 eV and $U_{\rm eff}^{(3+)}$=8.8 eV are shown in Fig. 4. For three divalent Yb ions the $4f$ bands are fully occupied and hybridize with As p states in the energy range between -0.5 and -2.5 eV. They are split due to spin-orbit coupling by $\Delta\epsilon_{so}$ =1.40 eV. For the trivalent Yb ion, thirteen $4f$ electron bands per ion are well below the Fermi level and separated from a $4f$ hole state by the correlation energy $U_{\rm eff}^{(3+)}$. One $4f$ hole band per Yb^{3+} ion, doubly degenerate due to AF ordering, appears closely below the top of the As p band. Since the As p band is separated from the Yb $5d$ band by an ordinary band gap, the Fermi level must be pinned at the bottom of the $4f$ hole band. This feature in combination with the small mass of the As p electrons close to the top of the p band appears to be a clue feature for the physics of the ytterbium pnictides.[52] Due to the very small phase space for hybridization and the very small Yb $4f$-As p orbital overlap, the DOS peak of the hole band is as narrow as 0.007 eV right above the Fermi level. It is now clear why the usual Kondo lattice scenario is inappropriate for these pnictide compounds. For a Kondo resonance to develop both the occupied and empty $4f$ states must be sufficiently far away from the Fermi level. Quite opposite to this situation, the (almost) empty level is pinned slightly above the Fermi energy. But due to the very small phase space for hybridization around the Γ point one still has an almost stable moment of the nearly integer occupation of the f shell.

The total DOS of the occupied part of the Yb_4As_3 band structure is compared with UPS measurements[21] in Fig. 5. The calculated DOS has been broadened to account for lifetime effects and for the experimental resolution. The As $4p$ states practically do not contribute to XPS and UPS because

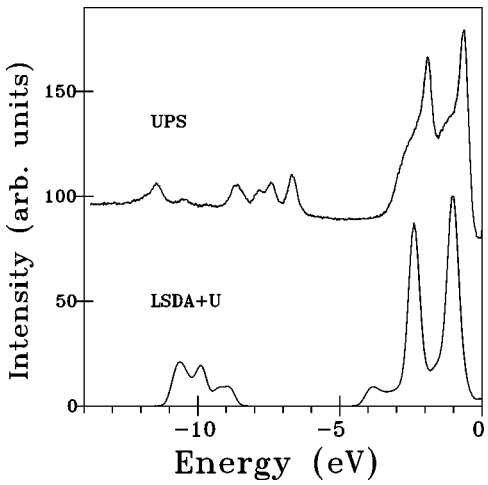

FIG. 5. Comparison between the calculated DOS as in Fig. 4 and the experimental UPS spectra from Ref. 21. The calculated DOS has been broadened according to experimental resolution.

of the low ionization cross section compared with that of the Yb $4f$ states.[53] Hence, the measurements only indicate the f excitation energies of trivalent and divalent Yb, relative to the Fermi level. The double-peak structure at 0.5 to 2.5 eV binding energy reflects the spin-orbit doublet of the $4f^{13}$ final states on Yb^{2+} sites. The humps towards higher binding energies from both peaks are usually interpreted as surface states.[20,21] The structures between 6 and 13 eV binding energy should be assigned to the multiplet structure of the $4f^{12}$ final states on Yb^{3+} sites. The LSDA+U DOS cannot, of course, fully account for this multiplet splitting. From this comparison we can only conclude that $U_{\rm eff}^{(2+)}$ should be between 5 and 6 eV, and that $U_{\rm eff}^{(3+)}$ should be between 7 and 10 eV. More specific conclusions on the value of $U_{\rm eff}^{(3+)}$ will be drawn below from other independent experiments, namely, the Hall coefficient, and optical and cyclotron resonance measurements. Before we address these, we focus again on the main issue of our analysis, which is rather little dependent on the precise value of $U_{\rm eff}^{(3+)}$.

Since the $4f$ binding energy of the Yb^{2+} ions is larger than 0.5 eV and hence larger than the Yb $4f$-As p orbital hybridization energy both in experiment and in our calculated band structure, the $4f$ shell of the Yb^{2+} ions has been treated as a core shell in the following detailed numerical analysis. It has been checked that this simplification does not affect the issue. Therefore, we are left with a charge balance between Yb $4f$ states of the Yb^{3+} ions and pnictide p states only. Any charge transfer between these states causes a change in the Hartree potential that is governed by the *bare Coulomb integral* U_f of the $4f$ state being as large as 30 eV. Thus, an artificial shift via tuning $U_{\rm eff}^{(3+)}$ of the hole f level by 3 eV, say, (corresponding to a change of $U_{\rm eff}^{(3+)}$ itself by 6 eV), will completely be compensated by a charge transfer as small as 0.1 electron charge. For this reason the $4f$ hole level, to which the Fermi level is pinned, is itself very rigidly pinned close to the top of the pnictide p band.

In Fig. 6 the band structure in the vicinity of the Fermi level is shown for $U_{\rm eff}^{(3+)}$=9.6 eV. It corresponds to a ground state with a hole pocket around the Γ point ($\boldsymbol{k}=0$) holding 0.0058 As p holes per formula unit. For chosen values

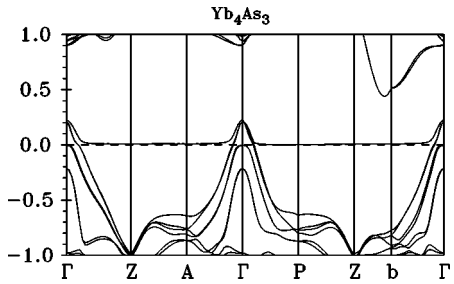

FIG. 6. Self-consistent LSDA+U energy band structure of Yb_4As_3 along the high-symmetry directions and for energies close to the Fermi level. (Here, $U_{\rm eff}^{(3+)}$=9.6 eV, and the f shell of the Yb^{2+} ions is treated as a core shell.)

$U_{\rm eff}^{(3+)}$=5.3, 7.0, 9.6, and 9.8 eV the obtained hole numbers are 0.0717, 0.0225, 0.0058, and 0.0005, respectively. Only for $U_{\rm eff}^{(3+)} \geqslant 10$ eV the As p band would be filled and the Fermi level would lie in a gap between this band and the f hole state. This *generic* feature is obtained independent of whether the filled f shell of the Yb^{2+} ions is treated as core or as valence, whether AF of ferromagnetic order is assumed on the Yb^{3+} chains, or whether spin-orbit coupling is taken into account or not, all the involved energies being small compared to the unscreened U_f. Figure 7 shows the obtained partial DOS close to the Fermi level for a number of cases.

The carrier density in Yb_4As_3 at low temperature is extremely low, for which the following findings give evidence: (1) a large value of the resistivity up to 10 mΩ,[1] (2) a very low plasma frequency obtained from optical reflectivity,[25] and (3) a large value of the Hall coefficient,[1] which corresponds to about 0.001 holes per Yb^{3+} ion, assuming the single carrier model. Yb_4As_3 is a compensated semimetal, so the number of As p holes exactly equals the number of excess Yb $4f$ electrons in the partially filled $4f$ hole level. However, the mobility of heavy $4f$ electrons is assumed to be negligible in comparison with the mobility of As p electrons.[1] So the transport properties of Yb_4As_3 are mostly determined by the number of As p holes.

In our analysis, a carrier number of 0.001 per formula unit would result from a $U_{\rm eff}^{(3+)}$ value between 9.6 and 9.8 eV which would not be in contradiction to photoemission. We would like to emphasize that we do not claim to explain the carrier number 0.001, but we claim to give an explanation why the carrier number is *small*.

The small mass at the top of the pnictide p band results in a very low p DOS of 0.015 states per eV, atom and spin, at the f hole level for $U_{\rm eff}^{(3+)}$=9.6 eV. That means that there are very few p-band states to broaden the f level by hybridization. The width of the hole state equals to about 0.007 eV (80 K) and decreases with increasing $U_{\rm eff}^{(3+)}$. The total DOS at the Fermi level, resulting essentially from the $4f$ hole states, yields for $U_{\rm eff}^{(3+)}$=9.6 eV a large band structure contribution to the Sommerfeld constant of $\gamma = \pi^2 k_B^2 N_A N(\epsilon_F)/3 = 40$ mJ mol^{-1} K^{-2}. The calculated γ is substantial, yet it corresponds only to the experimental value in a sufficiently strong magnetic field that suppresses magnetic moment fluctuations.[4] Since Yb_4P_3, although a semiconductor, has an

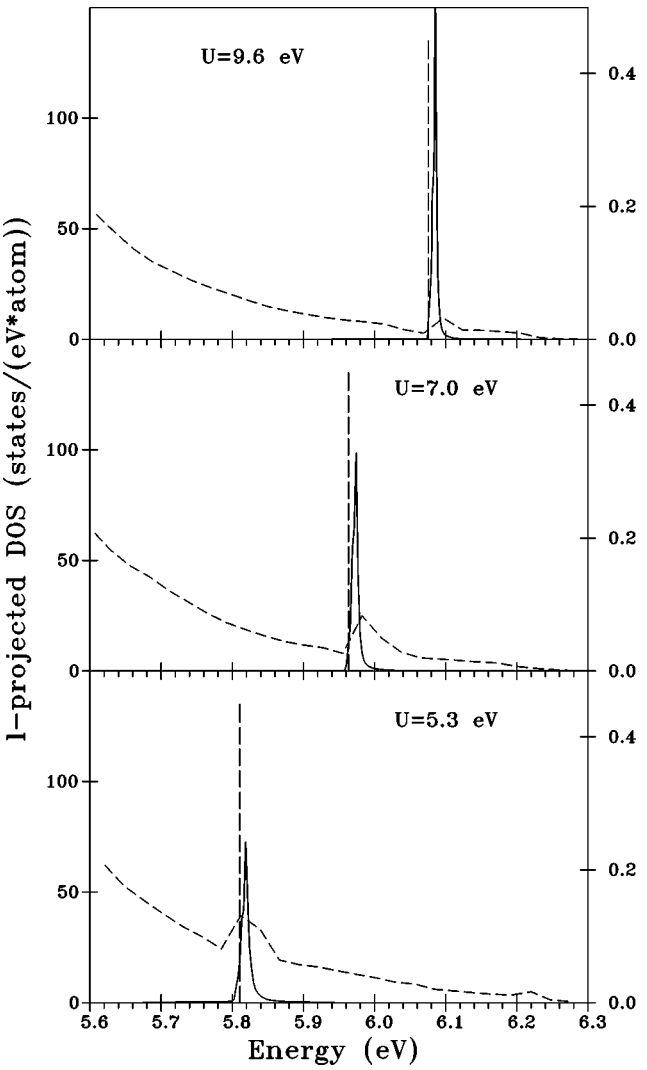

FIG. 7. Yb $4f$ partial DOS and As $4p$ partial DOS of Yb_4As_3 on an expanded energy scale around the Fermi level (dashed vertical line) for various values of $U_{\rm eff}^{(3+)}$. The left ordinate scale is for the f DOS and the right one for the p DOS.

even larger value of the Sommerfeld constant than Yb_4As_3, a large part of γ must be due to fluctuations of the magnetic moments in charge-ordered $\langle 111 \rangle$ chains. Beyond LSDA $+U$, further many-body interactions need to be invoked to account for the full Sommerfeld constant of the specific heat.[32,54]

B. Optical spectra of Yb_4As_3

While XPS and UPS cover a large excitation energy region, optical measurements (optical reflectivity) probe the electronic structure essentially at a few eV around the Fermi level. The linear response of a system to an external electromagnetic field is determined by the complex dielectric function ε.

We have calculated the dielectric function considering only electronic excitations. We used the random-phase approximation and neglected local-field and finite lifetime

effects.[55] The interband contribution to the imaginary part of the dielectric function is given by

$$\varepsilon_2(\omega)=\frac{4\pi^2e^2}{m^2\omega^2}\sum_{n}^{\text{unocc}}\sum_{n'}^{\text{occ}}\int_{\text{BZ}}|P_{nn'}(\boldsymbol{k})|^2 \times\delta(\epsilon_n^{\boldsymbol{k}}-\epsilon_{n'}^{\boldsymbol{k}}-\hbar\omega)\,\frac{d^3k}{(2\pi)^3}, \quad (2)$$

where $P_{nn'}(\boldsymbol{k})$ is the projection of the momentum matrix elements $P_{nn'}(\boldsymbol{k})$, and $\epsilon_n^{\boldsymbol{k}}$ are the electron band energies (one band per spin). The expressions for calculation of the optical transition matrix element in Dirac representation within LMTO formalism have been derived in Ref. 56.

After having evaluated Eq. (2) in a wide energy range from 0 to 40 eV, we have calculated the interband contribution to the real part of the dielectric function $\varepsilon_1(\omega)$ using the Kramers-Kronig relation. Finally, we have added the intraband contribution to obtain the total complex dielectric function. We neglect this contribution to $\varepsilon_2(\omega)$, assuming a perfect crystal and neglecting lattice vibrations. The intraband contribution to $\varepsilon_1(\omega)$ is given by $\varepsilon_1(\omega)_{\text{intra}}=1-\omega_p^2/\omega^2$, where the squared plasma frequency is given by

$$\omega_p^2=\frac{1}{2}\left(\frac{e}{\pi\hbar}\right)^2\sum_n\int_{\text{BZ}}d^3k[\partial\epsilon_n^{\boldsymbol{k}}/\partial k]^2\delta(\epsilon_n^{\boldsymbol{k}}-\epsilon_F). \quad (3)$$

We also calculated the reflectivity $R(\omega)$ using Eqs. (2) and (3) and the following relation: $R(\omega)=|(\sqrt{\varepsilon}-1)/(\sqrt{\varepsilon}+1)|^2$. The calculated values of the plasma frequencies are $\omega_p=1.21$ and 0.26 eV for $U_{\text{eff}}^{(3+)}=5.3$ and 9.6 eV, respectively (averaged values over polarization directions). The experimental value of ω_p varies from 0.08 eV at 10 K to 0.14 eV at 70 K.[25]

In Fig. 8 we compare the calculated complex dielectric function $\varepsilon(\omega)$ and the reflectivity $R(\omega)$ for $U_{\text{eff}}^{(3+)}=7.0$ and 9.6 eV with experiment.[23] As can be seen, theory and experiment agree fairly well for $U_{\text{eff}}^{(3+)}=9.6$ eV. For $U_{\text{eff}}^{(3+)}=7.0$ eV there is an additional As p band crossing the Fermi level near the Γ point. $U_{\text{eff}}^{(3+)}=9.6$ eV yields a very small carrier concentration, hence a small value of the plasma frequency and low intensity of interband transitions to unoccupied As p states is in good agreement with the Hall coefficient and optical measurements.

We mention that with increasing photon energy beyond the range presented in Fig. 8, the measured optical reflectivity decreases rapidly from a value of 0.2 at 0.3 eV to 0.05 at 8 eV.[23] The calculated reflectivity, however, has a rather flat behavior at a value of about 0.3 up to 12 eV. To clarify this disagreement between theory and experiment, ellipsometric measurements of the optical properties of Yb_4As_3 are highly desired.

C. Fermi surface of Yb_4As_3

Figure 6 shows the LSDA+U energy band structure of Yb_4As_3 for $U_{\text{eff}}^{(3+)}=9.6$ eV near the Fermi level. Because of the absence of inversion symmetry in the crystal structure, the spin degeneracy of the bands is lifted, when spin-orbit interaction is taken into account. Therefore, each band holds only one electron state per AF unit cell. As is, however, seen from Fig. 6, this spin splitting is completely negligible close to the Fermi level, and two pairs of almost degenerate energy bands cross the Fermi energy: a pair of As p bands close to their top and the pair of nearly dispersionless f bands. The corresponding two small sheets of the Fermi surface are a hole pocket of As p states centered at the Γ point and an electron ellipsoid of Yb f states centered on the symmetry line Γ-P (Fig. 9).

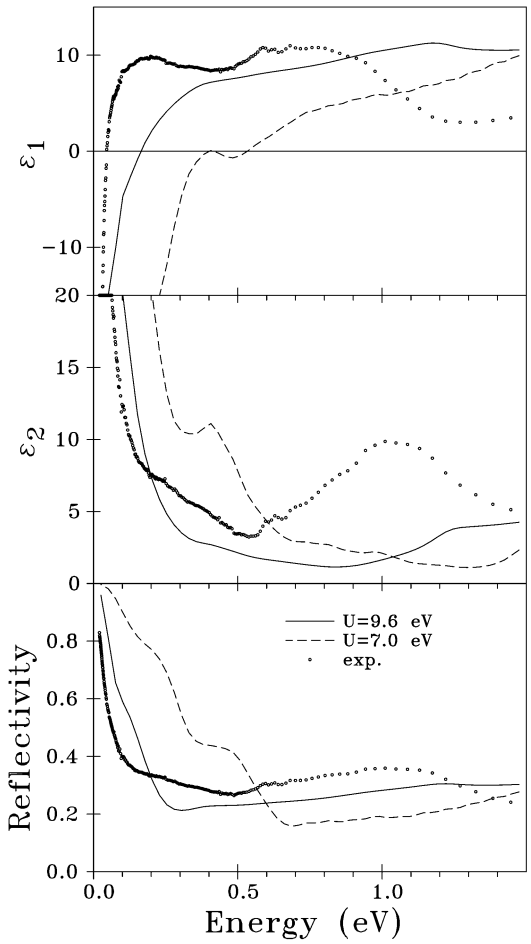

FIG. 8. Comparison between the experimental (Ref. 23) (dots) and calculated optical reflectivity R, the real part $\varepsilon_1(\omega)$ and the imaginary part $\varepsilon_2(\omega)$ of the dielectric function of Yb_4As_3 calculated with two different values of $U_{\text{eff}}^{(3+)}$: 7.0 eV (dashed line) and 9.6 eV (solid line).

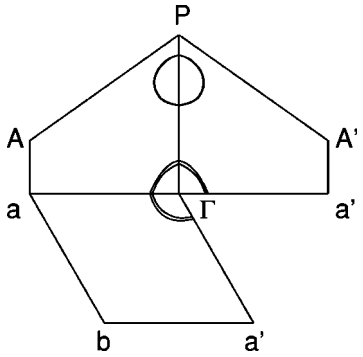

FIG. 9. Cross sections of the calculated Fermi surface of Yb_4As_3.

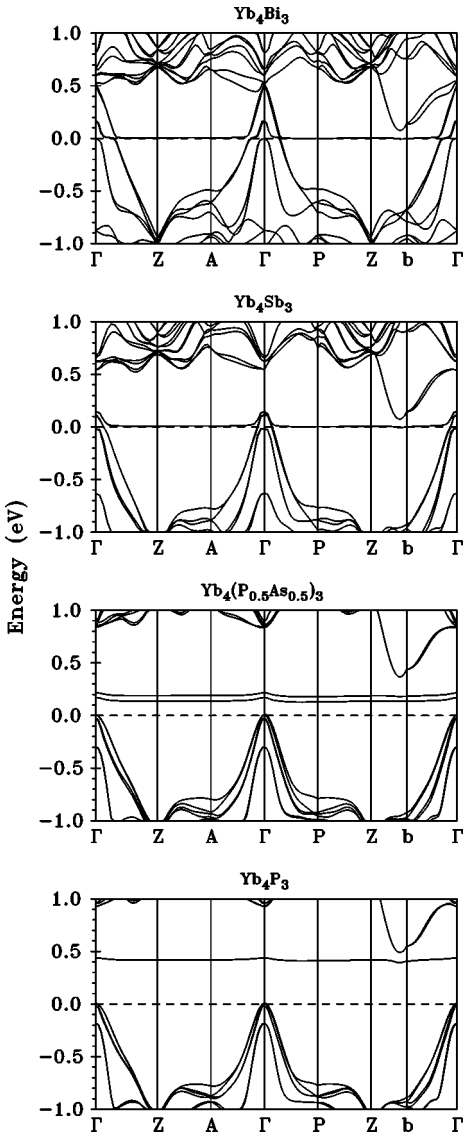

FIG. 10. Self-consistent LSDA+U ($U_{\text{eff}}^{(3+)}$=9.6 eV) energy band structure of Yb_4Bi_3, Yb_4Sb_3 (hypothetical $R3c$ symmetry), $Yb_4(P_{0.5}As_{0.5})_3$, and Yb_4P_3.

Both the hole and electron sheets of the Fermi surface are almost spherical. We have calculated the orientational dependence of the extremal cross sections and the cyclotron masses for several selected field directions. We found that the cyclotron masses for the hole sheet of As p states are in the range of 0.6 to 0.8 m_0, in rather good agreement with cyclotron resonance measurements ($m_{exp}=0.72m_0$), although the calculated band mass should be renormalized for the electron-phonon interaction. The cyclotron masses for the $4f$ band are obtained from the calculation as large as 36.1 to 38.8m_0. It seems not to be easy to detect a Fermi surface with such a large cyclotron mass experimentally. De Haas–van Alphen measurements of the Fermi surface of Yb_4As_3 are highly desirable to check whether the $4f$ electron sheet with this large effective mass exists.

D. Energy band structures of Yb_4P_3, Yb_4Sb_3, Yb_4Bi_3, and $Yb_4(P_{0.5}As_{0.5})_3$

Figure 10 shows the energy band structure and total density of states near the Fermi level for Yb_4P_3, Yb_4Sb_3, and Yb_4Bi_3 calculated in the trigonal $R3c$ AF crystal structure in the LSDA+U approximation with $U_{\text{eff}}^{(3+)}$=9.6 eV. We should mention that only Yb_4P_3 and Yb_4As_3 reveal the charge ordering cubic-to-trigonal structural transformation. The other two compounds remain in the cubic structure down to the lowest temperatures with the Yb^{3+} ions being randomly distributed among the four chains. Such a valence fluctuating system is presently outside the scope of our investigation.

TABLE I. The centers of gravity E_c relative to the Fermi energy and widths (in eV) of pnictogen np bands ΔE_{np} in Yb_4X_3 compounds.

Compound	E_c	ΔE_{np}
Yb_4P_3	−2.01	4.00
Yb_4As_3	−1.79	4.20
Yb_4Sb_3	−2.18	4.45
Yb_4Bi_3	−2.28	4.65

The main trend in the electronic structure of the sequence of Yb_4X_3 compounds (X=P, As, Sb, or Bi) results from the characteristic trend in the pnictide p wave functions and from the systematic change of the lattice parameters. The counteraction of screening by inner atomic shells and of relativistic effects leads to the characteristic trend in the position of the atomic p state and hence of the center of gravity of the pnictide p band, first increasing from P to As and then monotonically decreasing to Bi. The p-band width is monotonically increasing from P to Bi due to the increasing extension of the atomic wave function, although the lattice constant increases too (see Table I). Therefore, if one moves from Yb_4Bi_3 to Yb_4P_3 through the series, the unoccupied $4f$ level moves from below towards the top of the pnictide p band and beyond, implying a reduction of metalicity and finally a transition to semiconducting behavior, which is experimentally found in $Yb_4(As_{1-x}P_x)_3$ for $x \geqslant 0.4$ (Ref. 2). Figure 10 shows the energy band structure of the series, including also, $Yb_4(As_{0.5}P_{0.5})_3$. In this compound, treated as ordered, two AF ordered Yb^{3+} ions are no longer chemically equivalent and the system becomes ferrimagnetic. This leads to a splitting of the $4f$ hole bands. These bands are already well above the top of the valence band, in agreement with the experimental data.[2]

Experimentally, Yb_4Sb_3 and Yb_4Bi_3 show the typical valence fluctuating behavior.[1] Their energy band structures calculated for hypothetical trigonal $R3c$ symmetry differ significantly from that of Yb_4As_3. With the increasing pnictide p-band widths, already in Yb_4Sb_3 the indirect gap between the top of the Sb $5p$ valence band and the bottom of the Yb $5d$ conduction band is closed (Fig. 10). In Yb_4Bi_3 the direct gap has also disappeared due to further broadening of the Bi $6p$ conduction band. However, there is still no overlap between the partly filled narrow Yb $4f$ band and the Yb $5d$ conduction band in both compounds.

In order to separate the influence of the lattice constant from the influence of the ionic potential of the pnictide component on the electronic structure of Yb_4X_3 (X=P, As, Sb, and Bi), we present in Fig. 11 the electronic structure of

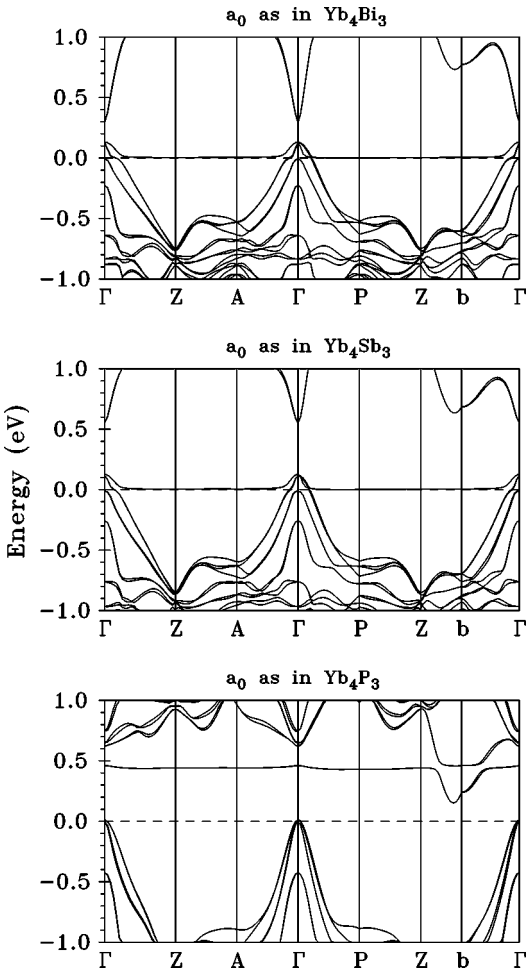

FIG. 11. Self-consistent LSDA+U ($U_{\text{eff}}^{(3+)}$=9.6 eV) energy band structure of Yb_4As_3, but with the lattice constants of Yb_4Bi_3, Yb_4Sb_3, and Yb_4P_3.

Yb_4As_3 calculated for lattice constants corresponding to those of Yb_4Bi_3, Yb_4Sb_3, and Yb_4P_3. The electronic structure of Yb_4As_3 with lattice parameters equal to those of the Yb_4Sb_3 and Yb_4Bi_3 compounds differs significantly from that of the real antimonide and bismuthide, respectively. In the energy-band structure of Yb_4As_3 with lattice constants of Yb_4Bi_3 there is still an energy gap between the top of the p valence band and the bottom of the Yb $5d$ conduction band. We can conclude that in the cases of the Yb_4Sb_3 and Yb_4Bi_3 compounds the type of pnictide ion potential plays an essential role due to its influence on the relative position and width of the p bands. We should mention that the real systems Yb_4Sb_3 and Yb_4Bi_3 are very complicated due to charge and moment fluctuations. More sophisticated methods are needed to investigate their electronic structure.

E. Charge ordering

Yb $4f$ electrons can hop from Yb site to Yb site only via pnictide sites since the direct f-f overlap is completely negligible. As long as there are enough pnictide p states available in the energy range of hybridization with the Yb $4f$ states, the hopping probability for the Yb $4f$ electron may suffice so that the $4f$ occupation number can fluctuate at each Yb site. This is the case in the cubic $I4\bar{3}d$ phases of Yb_4Sb_3 and Yb_4Bi_3. If this hopping is practically prohibited by a nearly vanishing pnictide p DOS as in Yb_4As_3 and Yb_4P_3, a charge separation into $Yb^{3+}Yb_3^{2+}X_3^{3-}$ follows. There are two competing rather simple structures into which this charge separation may order: a cubic $P2_13$ structure with a sequence

$$—Yb^{3+}—Yb^{2+}—Yb^{2+}—Yb^{2+}—Yb^{3+}—Yb^{2+}— \quad (4)$$

in each of the four families of chains (the Yb sites in this hypothetical $P2_13$ phase would have four inequivalent Wyckoff positions $4a$,.3., with $x_1 \ldots x_4$ along the chains. We again took the x values unshifted from the reference $I4\bar{3}d$ structure.), and the trigonal $R3c$ phase explained in the Introduction and in Sec. II. In both cases the self-consistent site charge difference between the Yb^{2+} and the Yb^{3+} ions is 0.2 electron charges, and it is natural to compute the difference in the Madelung energies of both structures. Independent of treating the pnictide ions as point charges or as homogeneous background, the Madelung energy of the cubic structure with chains (4) is 6 mRyd/(formula unit) lower than that of the trigonal structure. That the spatial distribution of the pnictide charges does not influence the considered Madelung energy *difference* is easily understood since all Yb sites are exactly symmetry equivalent with respect to the pnictide sublattice in the $I4\bar{3}d$ reference structure. Hence, they see exactly the same Madelung potential from the pnictide sublattice independently of how large it is. In order to go beyond Madelung energies, LSDA total energy calculations for Yb_4As_3 were performed with 14 and 13 Yb $4f$ electrons, respectively, put in the core. The numerical accuracy of the total energies was carefully checked to be better than 0.1 mRyd/(formula unit). These calculations yield a trigonal ground state with an energy by 2 mRyd/(formula unit) lower than that of the cubic phase. The total energy difference between ferromagnetic and antiferromagnetic order in the chain of the trigonal structure, which provides for an estimate of the interatomic magnetic coupling, is much smaller and amounts to 0.1 mRyd/(formula unit).

It is interesting to trace back which effect reverses the phase stability in favor of the trigonal phase against the Madelung contribution. By analyzing the self-consistent charges one finds a slight deviation of the charge of the middle of the three consecutive Yb^{2+} ions compared to the two others in the chain (4) of the cubic structure. Each Yb site of the structure of Fig. 1 has a first neighboring shell of six pnictide ions and a second neighboring shell of three Yb ions, each on one chain of the three other chain families seen from a chosen chain. Two adjacent Yb sites on the same chain are third neighbors of each other. Hence, in the trigonal structure where all Yb^{3+} ions are on one and the same chain family, an Yb^{2+} ion sees one Yb^{3+} ion and two Yb^{2+} ions in the second neighboring shell. All Yb^{2+} ions are symmetry equivalent. In the cubic structure of chains (4) on the other hand, the middle Yb^{2+} ion has three Yb^{3+} ions as second neighbors while the two others have only Yb^{2+} ions as second neighbors. There is a slight charge disproportionation between this middle Yb^{2+} ion and the other two Yb^{2+} ions due to their different second neighbor shells. This disproportionation costs 8 mRyd/(formula unit) to be added to the Madelung energy difference. The charge difference be-

tween the two symmetry inequivalent types of Yb^{2+} ions amounts to 0.05 electron charges.

IV. SUMMARY AND CONCLUSIONS

Using the LSDA+U approach to band-structure calculations with a U value adjusted to experiment but close to theoretical estimates, we have found a band gap between the As p band and the Yb $5d$ band in Yb_4As_3. As a consequence, a very narrow marginally occupied Yb^{3+} $4f$ hole band is pinned close to the top of the As p valence band via the charge balance between Yb and As, which is governed by the large ($\sim$30 eV) bare Coulomb integral of the Yb $4f$ state. The same charge balance pins the Fermi level close to the bottom of this $4f$ hole band that has a width of 0.007 eV (80 K). It leads to an extremely low carrier density in Yb_4As_3. The Fermi surface of Yb_4As_3 consists of two almost spherical sheets: a hole pocket of As p states with a relatively small effective mass, centered at the Γ point of the BZ, and an electron ellipsoid of Yb $4f$ states with a relatively heavy mass, centered on the symmetry line Γ-P.

The systematic trends in the position and width of the pnictide p band when going through the pnictogen group of the periodic table leads to a transition to semiconducting behavior towards the light pnictogen end with a charge-transfer gap between the pnictide p band and the Yb $4f$ state, and to an increasing carrier number and hence increasing metalicity with valence fluctuating Yb ions towards the heavy pnictogen end. Already in $Yb_4(As_{0.5}P_{0.5})_3$ semiconducting behavior is found. In Yb_4Sb_3 and in Yb_4Bi_3 the band gap between the pnictide p valence band and the Yb $5d$ conduction band is closed.

For Yb_4As_3, the LSDA+U band-structure calculations provide a two-band model of the electronic structure: (1) a wide, nearly fully occupied As $4p$ valence band and (2) a very narrow, marginally occupied Yb $4f$ band, very weakly hybridized with the As $4p$ band in a small $\boldsymbol{k}$ space region near the Γ point of the BZ (Fig. 6).

Pressure, doping etc. may slightly change the relative position of these two bands and hence strongly affected the low-carrier density and the transport properties. But the $4f$ shell of the Yb^{3+} ions is little influenced as long as the charge order is maintained.

In our LSDA+U band-structure calculations we treated the Yb_4X_3 compounds as ideal systems with perfect charge and AF order. The real situation is much more complicated. Yb_4As_3 shows no magnetic ordering down to a very low temperature of 0.2 K.[3] However, experimental evidence for existence of short range AF correlations was found.[11] An external magnetic field strongly affects the magnetic excitations suppressing the heavy-fermion properties of Yb_4As_3.[4] Going from Yb_4As_3 to Yb_4P_3, the number of Yb^{3+} ions increases, the degree of charge and AF ordering also increases,[18] and despite the decrease of the number of free carriers (Yb_4P_3 is a semiconductor) the heavy-fermion properties are more pronounced, which is reflected in the increasing value of the Sommerfeld constant γ from about 200 $mJ\,mol^{-1}\,K^{-2}$ in Yb_4As_3 to 250 $mJ\,mol^{-1}\,K^{-2}$ in Yb_4P_3. Going to heavier pnictogen ions, metalicity increases and the tendency to moment and charge order is lost, a typical mixed valence behavior is found instead.

The large γ value of the semimetal Yb_4As_3 cannot be incorporated into Landau's Fermi-liquid theory for the following reason. In Landau's theory it is essential that the linear specific heat coefficient γ is related to the density of states at the Fermi level that depends on the quasiparticle masses. This relation does not hold here as seen by realizing that a large γ value is found even in the absence of any Fermi surface like in $Yb_4(As_{1-x}P_x)_3$ for $x \geqslant 0.4$. This is not surprising as the huge γ value can be assigned to spin excitations in the Heisenberg chains and is therefore unrelated to the quasiparticle excitations near the Fermi surface. It depends on the characteristic energy for the fluctuations of magnetic moments in the charge ordered $\langle 111 \rangle$ f^{13} chains that are given by the superexchange of f^{13} moments along chains via pnictide orbitals. Note that only the effective moments of the lowest crystal-field doublets are relevant here. We speculate that, if the complete Fermi surface and the effective masses of Yb_4As_3 could be measured, one would find that they do not explain the specific heat in contradiction with Landau's Fermi-liquid theory. Therefore, this concept requires a generalization. One of the strong points of Landau's theory is that it is a phenomenological approach, which does not require a microscopic model for a given material. It is within that spirit that a generalization is suggested by postulating in addition to the charged fermions (electrons or holes) a liquid of neutral fermions with a density of states $N^*(0)$. This density of states is fitted to the γ value of the specific heat. The underlying physical picture is, of course, that the magnonlike spin excitations in the chains, although of bosonic character, can be transformed into charge neutral fermionic excitations giving rise to the large γ value. But, as pointed out above, we are dealing with a phenomenological theory, and therefore no microscopic justification of the postulate is required. A liquid of neutral fermions for the description of a metallic system was suggested before by Kagan *et al.*[57] in connection with Kondo lattices. In the present case, the neutral fermions do not contribute to electric transport, but, e.g., to the thermal conductivity. They contribute also to the compressibility and to the spin susceptibility. The observed $\rho(T) = AT^2$ behavior at low temperature[1] with $A = 0.75\ \mu\Omega\ cm/K^2$ has to be interpreted as resulting from the scattering of the charged quasiparticles off the neutral fermions. A more detailed analysis of these features is left for a future investigation.

ACKNOWLEDGMENTS

V.N.A., A.N.Y., A.Y.P., P.M.O., and H.E. acknowledge financial support from the Max Planck society to the MPG Research Unit ''Electron Systems'' where part of the work was done. V.N.A., A.N.Y., and A.Y.P. gratefully acknowledge the hospitality extended to them during their stay at the Max Planck Institute for the Physics of Complex Systems in Dresden. We would like to thank Shin-ichi Kimura for providing the measured optical spectra, and H.-G. von Schnering for stimulating discussions of the Madelung energy and of structural aspects. We also benefited from discussions with E. Katz and G. Khaliullin.

*Permanent address: Institute of Metal Physics, 36 Vernadskii str., 252142 Kiev, Ukraine.

†Permanent address: Max Planck Institute for Chemical Physics of Solids, D-01187 Dresden, Germany.

[1] A. Ochiai, T. Suzuki, and T. Kasuya, J. Phys. Soc. Jpn. **59**, 4129 (1990).

[2] A. Ochiai, H. Aoki, T. Suzuki, R. Helfrich, and F. Steglich, Physica B **230-232**, 708 (1997).

[3] P. Bonville, A. Ochiai, T. Suzuki, and E. Vincent, J. Phys. I **4**, 595 (1994).

[4] P. H. P. Reinders, U. Ahlheim, K. Fraas, F. Steglich, and T. Suzuki, Physica B **186-188**, 434 (1993); R. Helfrich, F. Steglich, and A. Ochai (private communication).

[5] T. Suzuki, Physica B **186-188**, 347 (1993).

[6] T. Suzuki, Jpn. J. Appl. Phys., Part 1 **8**, 267 (1993).

[7] A. Ochiai, D. X. Li, Y. Haga, O. Nakamura, and T. Suzuki, Physica B **186-188**, 437 (1993).

[8] T. Kasuya, J. Phys. Soc. Jpn. **63**, 2481 (1994).

[9] T. Suzuki, Jpn. J. Appl. Phys., Part 1 **8**, 44 (1993).

[10] M. O'Keeffe and S. Andersson, Acta Crystallogr., Sect. A: Cryst. Phys., Diffr., Theor. Gen. Crystallogr. **33**, 914 (1977).

[11] M. Kohgi, K. Iwasa, A. Ochiai, T. Suzuki, J.-M. Mignot, B. Gillon, A. Gukasov, J. Schweizer, K. Kakurai, M. Nishi, A. Dönni, and T. Osakabe, Physica B **230-232**, 638 (1997).

[12] T. Goto, Y. Nemoto, S. Nakamura, A. Ochiai, and T. Suzuki, Physica B **230-232**, 702 (1997).

[13] T. Suzuki *et al.*, Physica B **206-207**, 771 (1995).

[14] Y. Okunuki, N. Mori, A. Ochiai, Y. Haga, and T. Suzuki, J. Phys. Soc. Jpn. **64**, 533 (1995).

[15] N. Mori, H. Takahashi, Y. Sekine, A. Ochiai, Y. Haga, T. Suzuki, T. Kashiwakura, S. Nakai, and M. Nomura, Physica B **230-232**, 630 (1997).

[16] O. Nakamura, A. Oyamada, A. Ochiai, S. Kunii, T. Takeda, T. Suzuki, and T. Kasuya, J. Magn. Magn. Mater. **76, 77**, 293 (1988).

[17] H. Aoki, A. Ochiai, T. Suzuki, R. Helfrich, and F. Steglich, Physica B **230-232**, 698 (1997).

[18] H. Aoki, T. Suzuki, and A. Ochiai (unpublished).

[19] O. Nakamura, Y. S. Kwon, A. Ochiai, T. Takeda, T. Suzuki, and T. Kasuya, Physica B **163**, 638 (1990); O. Nakamura, N. Tominada, A. Ochiai, T. Suzuki, and T. Kasuya, *ibid.* **171**, 377 (1991).

[20] S. Suga, S. Ogawa, H. Namatame, M. Taniguchi, A. Kakizaki, T. Ishii, A. Fujimori, S.-J. Oh, H. Kato, T. Miyahara, A. Ochiai, T. Suzuki, and T. Kasuya, J. Phys. Soc. Jpn. **58**, 4534 (1989).

[21] S. Suga, A. Ochiai, T. Suzuki, T. Matsushita, T. Iwasaki, H. Harada, A. Kimura, M. Tsunekawa, T. Muro, H. Daimon, S. Imada, H. Namatame, M. Taniguchi, H. Ishii, T. Mijahara, T. Hanya, A. Sekiyama, and A. Fujimori (unpublished).

[22] Y. Saitoh, S. Suga, H. Matsubara, Y. Tsukikawa, Y. Mori, A. Oyamada, A. Ochiai, T. Suzuki, and T. Kasuya, J. Phys. Soc. Jpn. **60**, 4005 (1991).

[23] S. Kimura, M. Ikezawa, A. Ochiai, and T. Suzuki, J. Phys. Soc. Jpn. **65**, 3591 (1996).

[24] S. Kimura, A. Ochiai, and T. Suzuki, Physica B **230-232**, 705 (1997).

[25] Y. S. Kwon, A. Ochiai, H. Kitazawa, N. Sato, H. Abe, T. Nanba, M. Ikezawa, K. Takegahara, T. Suzuki, and T. Kasuya, J. Magn. Magn. Mater. **70**, 397 (1987).

[26] R. Pittini, M. Ikezawa, A. Ochiai, H. Aoki, and T. Suzuki, J. Magn. Magn. Mater. **177-181**, 345 (1998).

[27] H. Matsui, T. Yasuda, A. Ochia, H. Harima, H. Aoki, T. Suzuki, and N. Toyota, Physica B **246-247**, 460 (1998).

[28] K. Takegahara, H. Harima, and T. Kasuya, J. Magn. Magn. Mater. **52**, 307 (1985).

[29] K. Takegahara and Y. Kaneta, J. Phys. Soc. Jpn. **60**, 4009 (1991).

[30] H. Harima, J. Phys. Soc. Jpn. **67**, 37 (1998).

[31] T. Kasuya, J. Phys. Soc. Jpn. **63**, 843 (1994).

[32] P. Fulde, B. Schmidt, and P. Thalmeier, Europhys. Lett. **31**, 323 (1995).

[33] B. Schmidt, P. Thalmeier, and P. Fulde, Physica B **223-224**, 373 (1996).

[34] Y. M. Li, N. d'Ambrumenil, and P. Fulde, Phys. Rev. Lett. **78**, 3386 (1997).

[35] V. I. Anisimov, J. Zaanen, and O. K. Andersen, Phys. Rev. B **44**, 943 (1991).

[36] V. I. Anisimov, F. Aryasetiawan, and A. I. Lichtenstein, J. Phys.: Condens. Matter **9**, 767 (1997).

[37] J. P. Perdew and A. Zunger, Phys. Rev. B **23**, 5048 (1981).

[38] J. F. Janak, Phys. Rev. B **18**, 7165 (1978).

[39] H. Eschrig, *The Fundamentals of Density Functional Theory* (B. G. Teubner, Stuttgart, 1996), Sec. 4.5.

[40] L. Hedin and B. I. Lundqvist, J. Phys. C **4**, 2064 (1971).

[41] P. M. Oppeneer, V. N. Antonov, A. N. Yaresko, A. Ya. Perlov, and H. Eschrig, Phys. Rev. Lett. **78**, 4079 (1997).

[42] A. N. Yaresko, P. M. Oppeneer, A. Ya. Perlov, V. N. Antonov, T. Kraft, and H. Eschrig, Europhys. Lett. **36**, 551 (1996).

[43] O. K. Andersen, Phys. Rev. B **12**, 3060 (1975).

[44] V. N. Antonov, A. Ya. Perlov, A. P. Shpak, and A. N. Yaresko, J. Magn. Magn. Mater. **146**, 205 (1995).

[45] V. V. Nemoshkalenko, A. A. Krasovsky, V. N. Antonov, Vl. N. Antonov, U. Fleck, H. Wonn, and P. Ziesche, Phys. Status Solidi B **120**, 283 (1982).

[46] U. von Barth and L. Hedin, J. Phys. C **5**, 1692 (1972).

[47] P. E. Blöchl, O. Jepsen, and O. K. Andersen, Phys. Rev. B **49**, 16 223 (1994).

[48] O. Jepsen and O. K. Andersen, Solid State Commun. **9**, 1763 (1971).

[49] J. F. Herbst and J. W. Wilkins, in *Handbook of the Physics and Chemistry of Rare Earths*, edited by K. A. Gschneidner, L. Eyring, and S. Hüfner (North-Holland, Amsterdam, 1987), Vol. 10, p. 321.

[50] P. H. Dederichs, S. Blügel, R. Zeller, and H. Akai, Phys. Rev. Lett. **53**, 2512 (1984).

[51] V. I. Anisimov and O. Gunnarsson, Phys. Rev. B **43**, 7570 (1991).

[52] We mention that quite recently it was shown, on the basis of LSDA+U electronic structure calculations, that in YbBiPt a somewhat similar $4f$ hole level pinning occurs (Ref. 41). In YbBiPt, however, the $4f$ hole level becomes pinned right at the Fermi level, which leads to a huge band-structure contribution to the Sommerfeld constant γ.

[53] J. J. Yeh and I. Lindau, At. Data Nucl. Data Tables **32**, No. 1 (1985).

[54] P. Fulde, *Electron Correlations in Molecules and Solids* (Springer, Berlin, 1995).

[55] H. Ehrenreich and M. H. Cohen, Phys. Rev. **115**, 786 (1959).

[56] V. N. Antonov, A. I. Bagljuk, A. Ya. Perlov, V. V. Nemoshkalenko, Vl. N. Antonov, O. K. Andersen, and O. Jepsen, J. Low Temp. Phys. **19**, 494 (1993).

[57] Yu. Kagan, K. A. Kikoin, and N. V. Prokof'ev, Physica B **182**, 201 (1992).